Geophysical Prospecting
EAGE EUROPEAN ASSOCIATION OF GEOSCIENTISTS & ENGINEERS
Geophysical Prospecting, 2021, **69**, 1745–1760 doi: 10.1111/1365-2478.13134

A computational review of the line integral analytical formulation of the polyhedral gravity signal

Dimitrios Tsoulis* and Georgia Gavriilidou

Department of Geodesy and Surveying, Aristotle University of Thessaloniki, Thessaloniki, Greece

Received November 2020, revision accepted June 2021

ABSTRACT

The generally shaped polyhedron is a widely used model in gravity field modelling and interpretation. Its induced gravity signal – gravitational potential and its derivatives up to second order – has been studied extensively in the geophysical literature. The class of solutions with special interest is the one which leads to closed analytical expressions, as these offer an exact representation of the gravity signal of finite three-dimensional distributions while being at the same time linked to a flexible means of geometric modelling. Of the several mathematical algorithms available, the line integral approach involves no approximations and is, however, connected with certain singularities, occurring for specific relative positions of the computation point with respect to the polyhedral source. The present contribution analyses the algorithmic details of the polyhedral line integral approach focusing on its geometric and computational aspects. Following the definitions of the individual coordinate systems and the two-step application of the Gauss divergence theorem for each face and polygonal boundary of the source, the geometric insight of the algorithm is presented, which permits a deeper understanding of the significance of the involved numerical singular terms. An overview of the line integral analytical approach for the polyhedral gravity signal is presented with emphasis on its geometric and computational aspects. Matlab code and results for the two considered case studies, a prismatic source and asteroid Eros, are provided as electronic supplement.

Key words: Gravity, Computing aspects, Theory, Modelling, Mathematical formulation, Potential field.

INTRODUCTION

The study of the analytical formulation of the polyhedral gravity signal dates back to the second half of the nineteenth century and continues to attract original contributions to this date. Though the underlying mathematical tool is the application of the divergence theorem of Gauss, different methodologies emerge from the varying parameterization of both the attracting source and the adopted application strategy. Tsoulis (2003) provides a short historical overview of the most commonly cited contributions on the subject, from a much larger set of publications. One group of manuscripts concentrates on the potential function and its first-order derivatives, i.e. the gravitational attraction (e.g. Barnett, 1976; Pohánka 1988), and other contributions include the complete tensor of second-order derivatives, most relevant to gravity gradiometry, evaluated through different methodological paths (Okabe, 1979; Götze and Lahmeyer, 1988; Werner, 1994; Holstein and Ketteridge, 1996; Werner and Scheeres, 1997; Hansen, 1999; Singh and Guptasarma, 2001; Holstein, 2003).

The computation of the polyhedral gravity signal remains an active research topic that continues to attract new contributions focusing both on theoretical and computational aspects.

*Email: tsoulis@auth.gr

More recent additions to the related literature include new mathematical approaches that eliminate singularities or expand the analytical formulation to include non-homogeneous distributions (D'Urso, 2013, 2014; D'Urso and Trotta, 2017; Ren et al, 2018, 2020) as well as applications covering a wide variety of areas in geodesy, geophysics and astronomy (Schmidt et al, 2011; Bucha et al, 2016; Chanut et al, 2017; Fukushima, 2017; Jiang et al, 2018; Zhang and Chen, 2018; Benedek et al, 2018; Capponi et al, 2018; Saraswati et al, 2019; Vitale and Fedi, 2020).

The present contribution concentrates on the linear integral method of Petrovic (1996). This approach implements the straightforward application of the divergence theorem two times: a first application which transforms the three-dimensional expressions for the sought functionals into two-dimensional integrations over the individual polygonal faces and a subsequent application which leads to a set of line integrals defined over the individual segments. The method is linked to specific numerical singularities, that emerge from the intrinsic mathematical singularity occurring in the application of the divergence theorem for characteristic locations of the computation point with respect to the polyhedral source and requires the evaluation of corresponding correction terms (Tsoulis and Petrovic, 2001). The method provides closed analytical expressions for the potential function V, its first-order derivatives $V_x,\ V_y,\ V_z$ and the complete tensor of second-order derivatives V_{ij}, with $i,\ j = x, y, z$ denoting the coordinates of a local Cartesian coordinate system situated at the computation point (Tsoulis, 2012).

From a computational point of view, the line integral algorithm is based on the subsequent definition of local coordinate systems following the projection of the computation point first on the different polyhedral faces and then on each of the line segments building the polygonal boundary of the corresponding face. As the previously mentioned singularities are bound to appear in this procedure, basic element of the algorithm is the constant monitoring of the positions of the computation point and its projections with respect to the boundaries of the polyhedral source. The documentation of the basic algorithmic details of the line integral polyhedral approach is the scope of the following sections. Thereby, the derivations that lead to the analytical expressions for the sought functionals are omitted. We focus only on the evaluation of the final form of the analytical formulation for the polyhedral gravity signal. After presenting these expressions and providing the necessary notation definitions, the key implementation steps of the algorithm are presented, stressing their computational and geometric properties.

The included material provides a rigorous algorithmic and geometric documentation of the line integral formulation, focusing on all involved algorithmic controls, not previously included in the related references of the method. In order to determine whether numerical discrepancies are thereby introduced, the complete algorithm has been coded independently in a different programming environment (Matlab) than the existing Fortran software released by Tsoulis (2012). The extensive undertaken numerical tests for different test bodies demonstrate a numerical identification of the two codes for the ensemble of the polyhedral gravity signal functions in the order of the decimal digits precision level of the double-precision floating point format.

THE LINE INTEGRAL METHOD

With the term gravity signal we define here the ensemble of the functionals related to the gravitational potential function V and its up to second-order derivatives, which are induced by a given finite three-dimensional distribution. Thus, the sought functionals are

$$V = G\rho \iiint_U \frac{1}{l}\,\mathrm{d}U, \tag{1}$$

$$\mathbf{V}_i = \mathbf{F}_i = \left(\frac{\partial V}{\partial i}\right)\mathbf{e}_i = G\rho \iiint_U \frac{\partial}{\partial i}\left(\frac{1}{l}\right)\mathrm{d}U\,\mathbf{e}_i \quad (i = x,\ y,\ z), \tag{2}$$

$$V_{ij} = \left(\frac{\partial^2 V}{\partial i j}\right) = G\rho \iiint_U \frac{\partial^2}{\partial i j}\left(\frac{1}{l}\right)\mathrm{d}U \quad (i,\ j = x,\ y,\ z), \tag{3}$$

where G denotes Newton's gravitational constant, ρ an assumed constant density value for the entire distribution, U the volume of the distribution, $\mathbf{e}_i$ a local unit vector base located at the computation point, x, y, z, the coordinates of the corresponding coordinate system with origin the computation point P and l the distance between computation point and arbitrary space points.

Equations (1)−(3) define a total of 13 quantities, namely one for the potential, three for the first and nine for the second-order derivatives. However, for the gradiometric tensor there are only five linearly independent second-order derivatives. Thus, the total number of the sought functionals reduces to nine.

Though the detailed mathematical derivation of the analytical solutions of equations (1)−(3) will not be considered here, it falls under the scope of our study to present the basic geometric definitions of this procedure, also in the

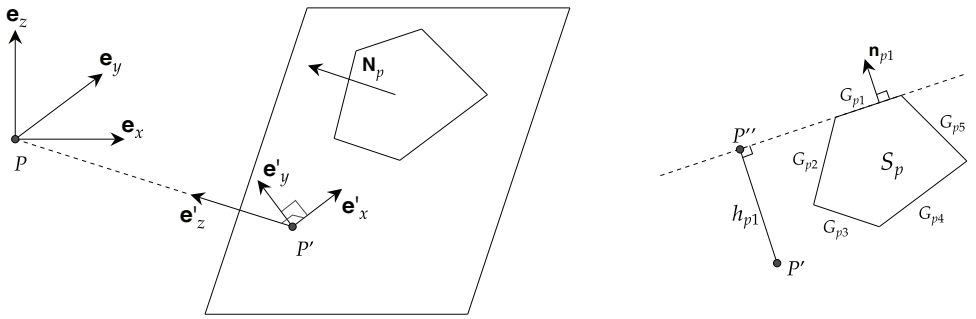

Figure 1 Notations related to the local coordinate system defined on face S_p.

context of the following section. Thus, the first step of the procedure involves the initial application of the Gauss divergence theorem, which transforms the volume integrations of equations (1)−(3) into a summation of surface integrals, one for each polyhedral face. Thereby, the computation point P is projected onto an equal number of projections P', one for every face. These projections are defined as the origins of new two-dimensional coordinate systems on the planes of the individual faces, that are used to describe the vertices and segments G_{pi} of the corresponding polygonal boundaries (Fig. 1). The index of segment G_{pi} describes its unique position in the topology of the considered three-dimensional distribution. Specifically, considering the numeration of the known topology which constructs uniquely the examined body, variable p stands for the number of the face containing the considered segment and variable i indicates the specific segment on that face.

The subsequent application of the divergence theorem takes place on the planes of the polyhedral faces and transforms the corresponding surface integrations into summations of line integrals equal to the number of segments defining each polygonal face. The obtained line integrals, have as limits the beginning and end points of the individual polygonal segments, while for the numerical description of these boundaries a further coordinate system definition is necessary, this time a one-dimensional one, defined along the direction of each segment and having as origin the projection P'' of point P' of that face onto the direction of the specific segment.

The definition of the last one-dimensional coordinate system along the polyhedral segments permits the analytical solution of the corresponding line integrals. This leads to the following final expressions for equations (1)–(3), respectively (Tsoulis, 2012):

$$V = \frac{G\rho}{2} \sum_{p=1}^{n} \sigma_p h_p \left[\sum_{q=1}^{m} \sigma_{pq} h_{pq} LN_{pq} + h_p \sum_{q=1}^{m} \sigma_{pq} AN_{pq} + \mathrm{SING}_{A_p} \right], \tag{4}$$

$$\mathbf{V}_i = G\rho \sum_{p=1}^{n} \cos\left(\mathbf{N}_p, \mathbf{e}_i\right) \left[\sum_{q=1}^{m} \sigma_{pq} h_{pq} LN_{pq} + h_p \sum_{q=1}^{m} \sigma_{pq} AN_{pq} + \mathrm{SING}_{A_p} \right] \mathbf{e}_i \tag{5}$$

$$= G\rho \Sigma_{p=1}^{n} \cos(\mathbf{N}_p, \mathbf{e}_i) \left[\Sigma_{q=1}^{m} \cos(\mathbf{n}_{pq}, \mathbf{e}_j) LN_{pq} + \sigma_p \cos(\mathbf{N}_p, \mathbf{e}_j) \Sigma_{q=1}^{m} \sigma_{pq} AN_{pq} + \mathrm{SING}_{B_{pj}} \right], \tag{6}$$

for $i,\ j = x,\ y,\ z$, where the following abbreviations are introduced:

$$LN_{pq} = \ln\left(\frac{s_{2pq} + l_{2pq}}{s_{1pq} + l_{1pq}}\right), \tag{7}$$

$$AN_{pq} = \arctan\left(\frac{h_p s_{2pq}}{h_{pq} l_{2pq}}\right) - \arctan\left(\frac{h_p s_{1pq}}{h_{pq} l_{1pq}}\right). \tag{8}$$

The polyhedral source is arbitrarily shaped, meaning it consists of a total of n polygonal faces, each defined by m segments, the latter number being able to vary between different faces. Thus, expressions (4)–(6) entail two kinds of summations: the one evolving over segments, the other over faces. $\mathbf{N}_p$ and $\mathbf{n}_{pq}$ denote unit vectors normal to the plane p and

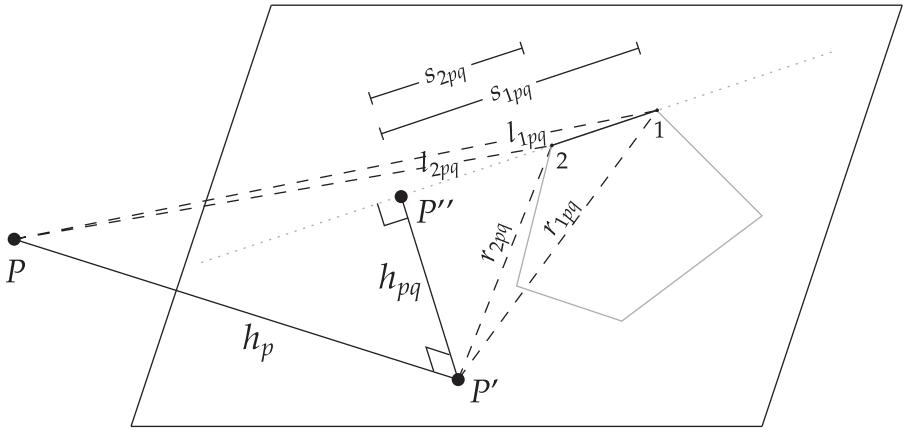

Figure 2 Involved parameters denoting different lengths in the line integral method.

segment pq laying on that plane respectively, σ_p and σ_{pq} are indicators of the relative positions of points P and P' with respect to the directions of $\mathbf{N}_p$ and $\mathbf{n}_{pq}$ respectively, obtaining the value of $+1$ when points P and P' are contained respectively in the half space and half plane towards which vectors $\mathbf{N}_p$ and $\mathbf{n}_{pq}$ are pointing, equalling to -1 otherwise. The rest of the involved parameters denote distances between points P, P' and P'' and the polyhedral vertices and are shown in Figure 2. Finally, quantities SING_{A_p} and $\mathrm{SING}_{B_{pj}}$ express the correction terms that need to be accounted for in case the positions of P, P' or P'' with respect to the polyhedral source lead to mathematical singularities of the divergence theorem and are discussed in Tsoulis and Petrovic (2001).

ALGORITHMIC ASPECTS AND GEOMETRIC IMPLICATIONS

The numerical evaluation of equations (4)–(6) requires as input data the coordinates of all polyhedral vertices with respect to the location of the computation point accompanied with the geometric topology of the source, which dictates the connectivity of the vertices. With this information the evaluation of all basic vectors can be performed directly. These include the vectors describing all segments as well as the outward-pointing unit normal vectors to each face and segment of the general polyhedron.

Computation of P' coordinates and position

In order to utilize the coordinate determination of points P', it is necessary to evaluate first the distances between computation point P and every plane defined by the individual polyhedral faces. This evaluation is facilitated by the Hessian plane equation form, which reads

$$Ax + By + Cz + D = 0. \tag{9}$$

If coefficients A, B, C, D are known, then the distance h_p to the plane described by (9) from the origin of the local coordinate system, which in our case coincides with point P, is defined as

$$h_p = \frac{D}{\sqrt{A^2 + B^2 + C^2}}. \tag{10}$$

For the computation of these coefficients, we examine three known points that define the considered plane adding an arbitrary point of the plane that enables its parameterization. Let $P_1(x_1, y_1, z_1)$, $P_2(x_2, y_2, z_2)$, $P_3(x_3, y_3, z_3)$ be three known polyhedral vertices that belong to the polygonal boundary of the specific face and $R(x, y, z)$ an additional point of the same plane. The geometric condition that links these four points is that the volume of the parallelepiped defined by them equals to zero, since they all belong to the same plane. This condition reads

$$\mathbf{P_1R} \cdot (\mathbf{P_1P_2} \times \mathbf{P_1P_3}) = 0, \tag{11}$$

which can be equally written in the form of the following determinant:

$$\begin{Vmatrix} x - x_1 & y - y_1 & z - z_1 \\ x_2 - x_1 & y_2 - y_1 & z_2 - z_1 \\ x_3 - x_1 & y_3 - y_1 & z_3 - z_1 \end{Vmatrix} = 0. \tag{12}$$

Developing this determinant we obtain the equation of the plane as

$$(x - x_1) \begin{Vmatrix} y_2 - y_1 & z_2 - z_1 \\ y_3 - y_1 & z_3 - z_1 \end{Vmatrix} - (y - y_1) \begin{Vmatrix} x_2 - x_1 & z_2 - z_1 \\ x_3 - x_1 & z_3 - z_1 \end{Vmatrix}$$

$$+ (z - z_1) \begin{Vmatrix} x_2 - x_1 & y_2 - y_1 \\ x_3 - x_1 & y_3 - y_1 \end{Vmatrix} = 0. \quad (13)$$

Thus, coefficients A, B, C, D become

$$A = \begin{Vmatrix} y_2 - y_1 z_2 - z_1 y_3 - y_1 z_3 - z_1 \end{Vmatrix} = (y_2 - y_1)\ (z_3 - z_1) - (z_2 - z_1)\,(y_3 - y_1), \quad (14)$$

$$B = \begin{Vmatrix} x_2 - x_1 z_2 - z_1 x_3 - x_1 z_3 - z_1 \end{Vmatrix} = (x_2 - x_1)\ (z_3 - z_1) - (z_2 - z_1)\,(x_3 - x_1), \quad (15)$$

$$C = \begin{Vmatrix} x_2 - x_1 y_2 - y_1 x_3 - x_1 y_3 - y_1 \end{Vmatrix} = (x_2 - x_1)\ (y_3 - y_1) - (y_2 - y_1)\,(x_3 - x_1), \quad (16)$$

$$D = -x_1 A + y_1 B - z_1 C. \quad (17)$$

Key parameter for the coordinates and position of P' is the plane unit normal vector $\mathbf{N}_p$, which for any given plane is computed through any two given segment vectors of that specific polyhedral face as

$$\mathbf{N}_p = \frac{\mathbf{G}_{i1} \times \mathbf{G}_{i2}}{\|\mathbf{G}_{i1} \times \mathbf{G}_{i2}\|}, \quad (18)$$

where $\mathbf{G}_{i1}$, $\mathbf{G}_{i2}$ are any two adjacent segments belonging to face i. Vector $\mathbf{N}_p$, when expressed in the common local coordinate system, is given by

$$\mathbf{N}_p = N_1\ \mathbf{e}_x + N_2 \mathbf{e}_y + N_3 \mathbf{e}_z \quad (19)$$

with its three components expressing the orientation of $\mathbf{N}_p$ with respect to base vectors $\mathbf{e}_x, \mathbf{e}_y, \mathbf{e}_z$, respectively. They are its direction cosines and can be seen as the sign allocators for the coordinates of each P'. In other words, it holds

$$N_1 = \cos\left(\mathbf{N}_p, \mathbf{e}_x\right), \quad (20)$$

$$N_2 = \cos\left(\mathbf{N}_p, \mathbf{e}_y\right), \quad (21)$$

$$N_3 = \cos\left(\mathbf{N}_p, \mathbf{e}_z\right). \quad (22)$$

Through vector $\mathbf{N}_p$ we are also able to compute the value for parameter σ_p for each plane, which expresses the relative position of P with respect to $\mathbf{N}_p$. By evaluating the inner product between $\mathbf{N}_p$ and any position vector of a vertex belonging to the specific polyhedral plane, we get the cases

$$\mathbf{N}_p \cdot \left(-\mathbf{G}_{p1}\right) = \begin{cases} > 0\ \sigma_p = -1 \\ < 0\ \sigma_p = +1 \\ = 0\ \sigma_p = 0 \end{cases} \quad (23)$$

which identify whether P is included in the half space pointed by $\mathbf{N}_p$, if it is situated in the other half space or if it lies on the specific plane, respectively (Fig. 3).

Now, the position of point P' on the specific plane can be evaluated as

$$x_{p'_i} = \pm\ \left\|\cos(\mathbf{N}_{p_i}, \mathbf{e}_x) h_{p_i}\right\|, \quad (24)$$

$$y_{p'_i} = \pm\ \left\|\cos\left(\mathbf{N}_{p_i}, \mathbf{e}_y\right) h_{p_i}\right\|, \quad (25)$$

$$z_{p'_i} = \pm\ \left\|\cos(\mathbf{N}_{p_i}, \mathbf{e}_z) h_{p_i}\right\|. \quad (26)$$

For the determination of the signs of $x_{p'_i}, y_{p'_i}, z_{P'_i}$ a further geometric investigation has to be carried out using the direction cosines of plane unit normal vectors $\mathbf{N}_p$ and the intersections of each polygonal plane with the three coordinate axes. If we denote with N_1, N_2, N_3 the three direction cosines of $\mathbf{N}_p$, and with $\alpha = -D/A$, $\beta = -D/B$, $\gamma = -D/C$ the intersections of the specific plane with axes $x,\ y,\ z$, respectively, we distinguish between following cases (Fig. 4):

Case A: $\alpha \geq 0,\ \beta \geq 0$ *and* $\gamma \geq 0$. In this case, all three coordinates $x,\ y,\ z$ of P' have positive values; thus, it will hold $x_{p'} = \|N_1 h_p\ \|, y_{p'} = \|N_2 h_p\ \|, z_{p'} = \|N_3 h_p\ \|$.

Case B: $\alpha < 0,\ \beta < 0$ *and* $\gamma < 0$. Here, all coordinates of P' must be controlled. We will have $x_{p'} = -N_1 h_p$ for $N_1 > 0$ or $x_{p'} = N_1\ h_p$ for $N_1 < 0$, $y_{p'} = -N_2 h_p$ for $N_2 > 0$ or $y_{p'} = -N_2 h_p$ for $N_2 < 0$ and $z_{p'} = -N_3 h_p$ for $N_3 > 0$ or $z_{p'} = N_3\ h_p$ for $N_3 < 0$.

Case C: $\alpha < 0$ *and* $\beta < 0$. In that occurrence, we get $\gamma > 0$ as the opposite sign for γ has been considered in case B. Here we have $x_{p'} = -N_1 h_p$ for $N_1 > 0$ or $x_{p'} = N_1\ h_p$ for $N_1 < 0$, $y_{p'} = -N_2 h_p$ for $N_2 > 0$ or $y_{p'} = N_2\ h_p$ for $N_2 < 0$ and $z_{p'} = \|N_3 h_p\ \|$.

Case D: $\beta < 0$ *and* $\gamma < 0$. We have $x_{p'} = \|N_1 h_p\ \|, y_{p'} = -N_2 h_p$ for $N_2 > 0$ or $y_{p'} = N_2\ h_p$ for $N_2 < 0$ and $z_{p'} = -N_3 h_p$ for $N_3 > 0$ or $z_{p'} = N_3\ h_p$ for $N_3 < 0$.

Case E: $\alpha < 0$ and $\gamma < 0$. It holds $x_{p'} = -N_1 h_p$ for $N_1 > 0$ or $x_{p'} = N_1\ h_p$ for $N_1 < 0$, $y_{p'} = \|N_2 h_p\ \|$ and $z_{p'} = -N_3 h_p$ for $N_3 > 0$ or $z_{p'} = N_3\ h_p$ for $N_3 < 0$.

Case F: $\alpha < 0$. In this case, we get $\beta > 0$ and $\gamma > 0$ as the opposite signs have already been considered. We will have $x_{p'} = -N_1 h_p$ for $N_1 > 0$ or $x_{p'} = N_1\ h_p$ for $N_1 < 0$, $y_{p'} = \|N_2 h_p\ \|$ and $z_{p'} = \|N_3 h_p\ \|$.

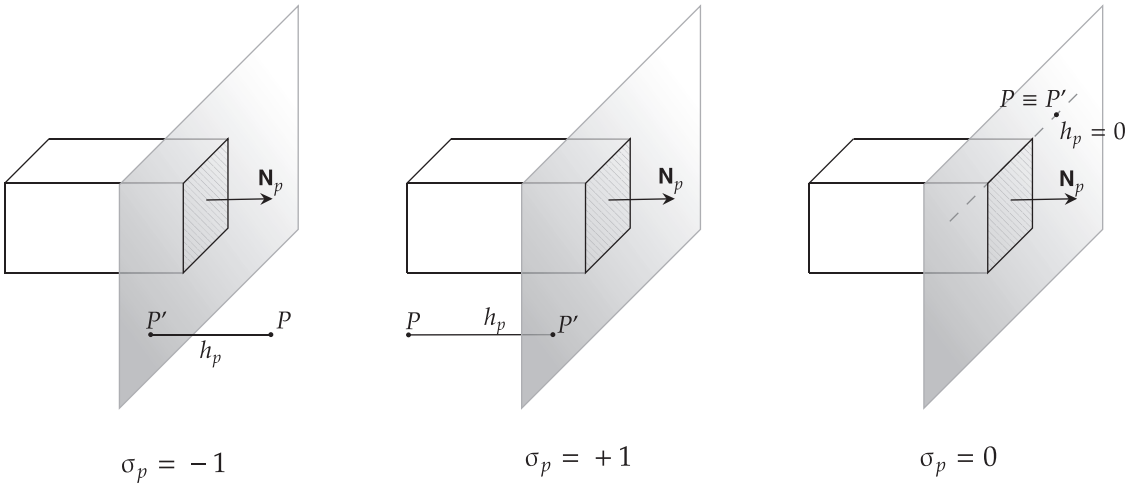

Figure 3 Possible relative positions of computation point P with respect to a specific polyhedral face.

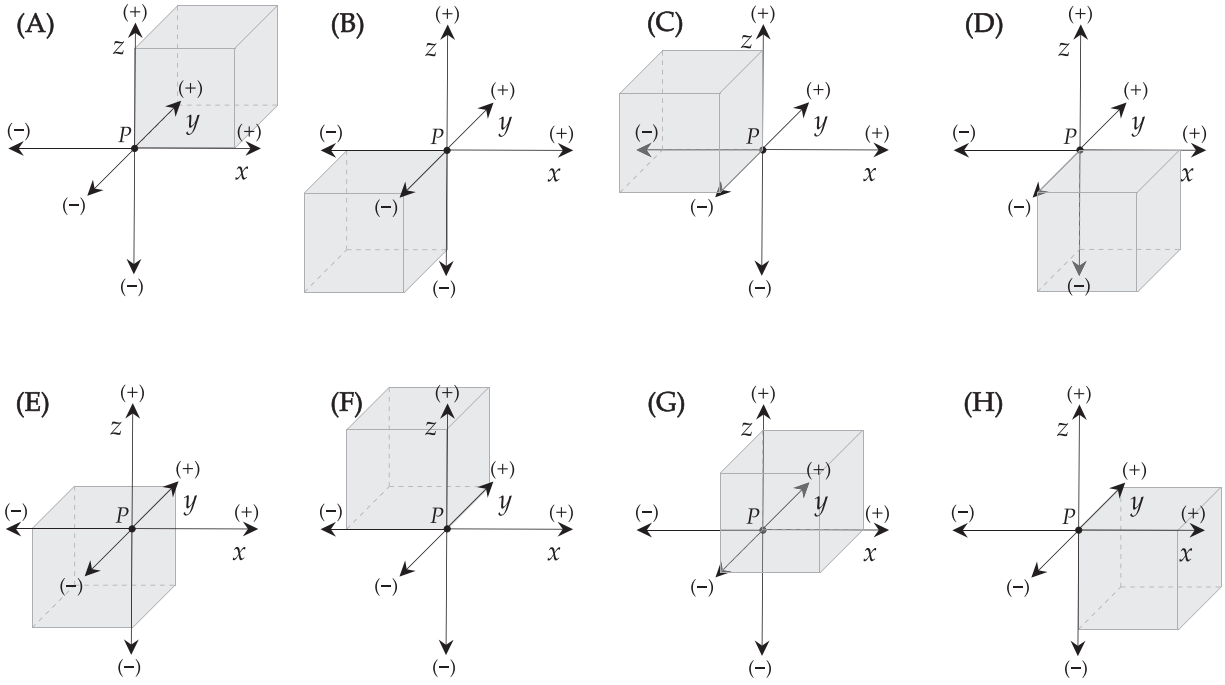

Figure 4 Different positions of point P' *with respect to the three axes of the local coordinate system situated at*P.

Case G: $\beta < 0$. Following the reasoning of case F we get $x_{p'} = \|N_1 h_p\|$, $y_{p'} = -N_2 h_p$ for $N_2 > 0$ or $y_{p'} = N_2 h_p$ for $N_2 < 0$ and $z_{p'} = \|N_3 h_p\|$.

Case H: $\gamma < 0$. Here we have $x_{p'} = \|N_1 h_p\|$, $y_{p'} = \|N_2 h_p\|$ and $z_{p'} = -N_3 h_p$ for $N_3 > 0$ or $z_{p'} = N_3 h_p$ for $N_3 < 0$.

Computation of *P″* coordinates and position

In the second application of the divergence theorem, this time on the plane of the considered polyhedral face, coefficients σ_{pq} have to be determined for every single segment. Similar to σ_p, an appropriate inner product can determine the relative

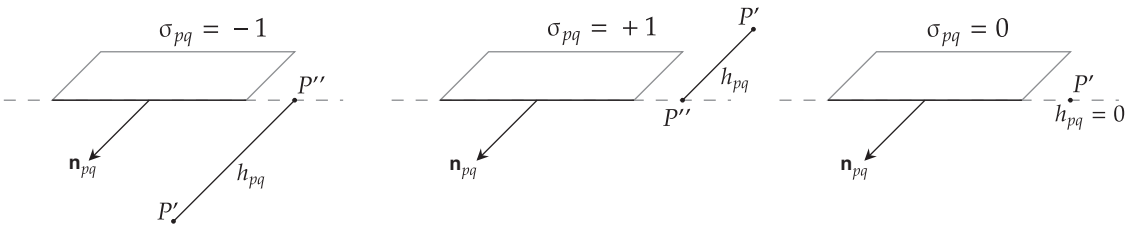

Figure 5 Possible relative positions of points P' *and*P'' *with respect to the corresponding segment.*

position of P'' with respect to the half plane pointed by segment unit normal $\mathbf{n}_{pq}$:

$$\mathbf{n}_{pq} = \frac{\mathbf{G}_{pq} \times \mathbf{N}_p}{\left\| \mathbf{G}_{pq} \times \mathbf{N}_p \right\|}. \tag{27}$$

If we denote with $\mathbf{x}_{p'}$ and $\mathbf{x}^1_{pq}$, respectively, the position vectors of P' and the first vertex of segment pq in the common coordinate system situated at P, the following three special cases are possible (Fig. 5):

$$\mathbf{n}_{pq} \cdot \left(\mathbf{x}_{p'} - \mathbf{x}^1_{pq} \right) = \begin{cases} > 0 \ \sigma_{pq} = -1 \\ < 0 \ \sigma_{pq} = +1 \\ = 0 \ \sigma_{pq} = 0 \end{cases} \tag{28}$$

The coordinate computation of points P'' results from the projection of the corresponding point P' on the different polyhedral edges of that plane. This computation is facilitated by building a system of three equations with involved unknowns the coordinates $x,\ y,\ z$ of each P''. The equations can emerge from the examination of specific geometric properties of vectors that include the unknown coordinates and lead to the construction of the required system of equations (Tsoulis, 2012). We extend here these considerations by providing the accompanied geometric context and methodological aspects.

First condition: Employed are segment vector $\mathbf{G}_{ij}$ and position vectors $\mathbf{x}'$ and $\mathbf{x}$ of projections P' and P'', respectively. The two position vectors are given in terms of the coordinates of the two points in the common coordinate system defined at the computation point P as

$$\mathbf{x}' = x_{p'}\mathbf{e}_x + y_{p'}\mathbf{e}_y + z_{p'}\mathbf{e}_z, \tag{29}$$

$$\mathbf{x} = x_{p''}\mathbf{e}_x + y_{p''}\mathbf{e}_y + z_{p''}\mathbf{e}_z. \tag{30}$$

If we subtract these vectors, the resulting vector $(\mathbf{x}' - \mathbf{x})$ has as origin point P'' for that particular segment and ends at point P' of that face (Fig. 6). Since P'' is per definition the projection of P' on the segment, vector $(\mathbf{x}' - \mathbf{x})$ will be normal to vector $\mathbf{G}_{ij}$; thus, their inner product will equal zero. This leads to the first equation

$$(\mathbf{x}' - \mathbf{x}) \cdot \mathbf{G}_{ij} = 0 \tag{31}$$

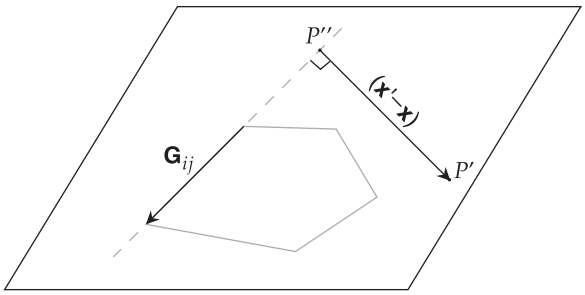

Figure 6 Geometric representation of the first condition for the retrieval of the coordinates of point P''.

which entails only coordinates $x_{p''},\ y_{p''},\ z_{p''}$ as unknowns. Indeed, equation (31) can be written as

$$\mathbf{x}' \cdot \mathbf{G}_{ij} = \mathbf{x} \cdot \mathbf{G}_{ij}, \tag{32}$$

If we consider that, when vector $\mathbf{G}_{ij}$ is written in the form,

$$\mathbf{G}_{ij} = a_1\ \mathbf{e}_x + b_1\mathbf{e}_y + c_1\mathbf{e}_z, \tag{33}$$

all vector components $a_1, b_1,\ c_1$ are known quantities, computed from the known coordinates of the two segment vertices, equation (32) becomes

$$d_1 = x_{p''}\ a_1 + y_{p''}b_1 + z_{p''}c_1 \tag{34}$$

with

$$d_1 = \mathbf{x}' \cdot \mathbf{G}_{ij} \tag{35}$$

being also a concrete numerical quantity, as the coordinates of point P' are already obtained from the previous step.

Second condition: Let us now introduce a further vector $\mathbf{y}$, which begins at P' and ends at the first vertex of the considered segment. It will hold

$$\mathbf{y} = \left(x^1_{ij} - x_{p'} \right)\ \mathbf{e}_x + \left(y^1_{ij} - y_{p'} \right)\mathbf{e}_y + \left(z^1_{ij} - z_{p'} \right)\mathbf{e}_z, \tag{36}$$

where $x^1_{ij},\ y^1_{ij},\ z^1_{ij}$ are the coordinates of the first vertex in the considered segment. The cross product between vectors $\mathbf{G}_{ij}$ and $\mathbf{y}$ defines a vector perpendicular to the plane where that particular segment belongs. Thus, it will also be normal to

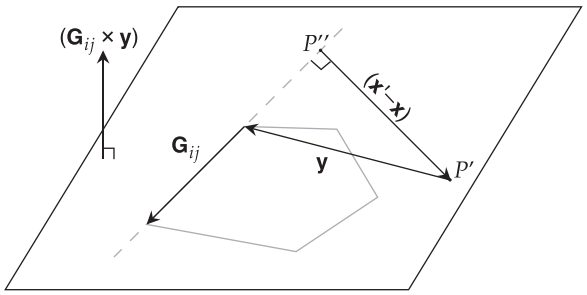

Figure 7 Geometric representation of the second condition for the retrieval of the coordinates of point P''.

any other vector that lies on that surface, for instance vector $(\mathbf{x}' - \mathbf{x})$ of the first condition. Consequently, the inner product between $(\mathbf{G}_{ij} \times \mathbf{y})$ and $(\mathbf{x}' - \mathbf{x})$ will be equal to zero, due to the fact that these two vectors are perpendicular (Fig. 7), and we will have

$$(\mathbf{x}' - \mathbf{x}) \cdot (\mathbf{G}_{ij} \times \mathbf{y}) = 0 \tag{37}$$

and finally

$$\mathbf{x}' \cdot (\mathbf{G}_{ij} \times \mathbf{y}) = \mathbf{x} \cdot (\mathbf{G}_{ij} \times \mathbf{y}). \tag{38}$$

The left-hand side of equation (38) is a real number which can be directly evaluated via the known components of all involved vectors. If we express the cross product $(\mathbf{G}_{ij} \times \mathbf{y})$ in a component form

$$\mathbf{G}_{ij} \times \mathbf{y} = \alpha_2 \, \mathbf{e}_x + b_2 \mathbf{e}_y + c_2 \mathbf{e}_z \tag{39}$$

a_2, b_2, c_2 will be known numerical quantities. Now, equation (38) becomes the second equation for the computation of the P'' coordinates

$$d_2 = x_{p''} \, a_2 + y_{p''} b_2 + z_{p''} c_2 \tag{40}$$

with

$$d_2 = \mathbf{x}' \cdot (\mathbf{G}_{ij} \times \mathbf{y}) \tag{41}$$

expressing a known numerical quantity.

Third condition: Finally, let $\mathbf{x}_1$ be the position vector of the starting point of each considered segment, i.e. it will hold

$$\mathbf{x}_1 = \left(x_{ij}^1\right) \, \mathbf{e}_x + \left(y_{ij}^1\right) \mathbf{e}_y + \left(z_{ij}^1\right) \mathbf{e}_z \tag{42}$$

with $x_{ij}^1, y_{ij}^1, z_{ij}^1$ the known coordinates of the origin of the considered segment. Vector $(\mathbf{x} - \mathbf{x}_1)$ begins at the first vertex of the segment and ends at the unknown point P''. This new vector belongs to the plane of the examined polyhedral face and lies on the direction of the segment. From the second condition, it is already shown that $(\mathbf{G}_{ij} \times \mathbf{y})$ is a vector perpendicular to the plane of the polyhedral face. Thus, the cross product

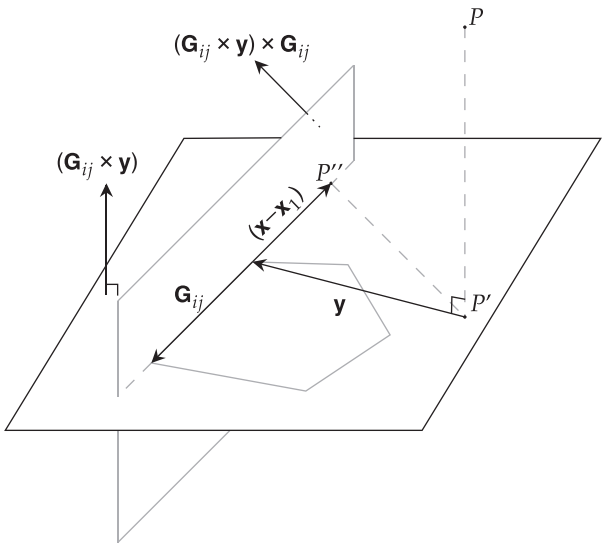

Figure 8 Geometric representation of the third condition for the retrieval of the coordinates of point P''.

between $(\mathbf{G}_{ij} \times \mathbf{y})$ and $\mathbf{G}_{ij}$ defines a new vector that is normal to the plane defined by vectors $(\mathbf{G}_{ij} \times \mathbf{y})$ and $\mathbf{G}_{ij}$. In turn, this fact dictates that vector $(\mathbf{G}_{ij} \times \mathbf{y}) \times \mathbf{G}_{ij}$ will be perpendicular to the segment vector and consequently perpendicular to vector $(\mathbf{x} - \mathbf{x}_1)$ as well (Fig. 8). From the above considerations, the third geometric condition, which will lead to the third equation for the determination of the coordinates for point P'', results from the fact that the inner product between vectors $(\mathbf{G}_{ij} \times \mathbf{y}) \times \mathbf{G}_{ij}$ and $(\mathbf{x} - \mathbf{x}_1)$ will be equal to zero. This reads

$$(\mathbf{x} - \mathbf{x}_1) \cdot \left((\mathbf{G}_{ij} \times \mathbf{y}) \times \mathbf{G}_{ij}\right) = 0 \tag{43}$$

and finally

$$\mathbf{x}_1 \cdot \left((\mathbf{G}_{ij} \times \mathbf{y}) \times \mathbf{G}_{ij}\right) = \mathbf{x} \cdot \left((\mathbf{G}_{ij} \times \mathbf{y}) \times \mathbf{G}_{ij}\right) \tag{44}$$

where the left-hand side defines a known scalar value, namely

$$d_3 = \mathbf{x}_1 \cdot \left((\mathbf{G}_{ij} \times \mathbf{y}) \times \mathbf{G}_{ij}\right). \tag{45}$$

The right-hand side contains the sought coordinates of P'' and the double cross product in parentheses, which is a known vector, as it is defined by known quantities. In other words, the expression in question can be written in the following form:

$$\left((\mathbf{G}_{ij} \times \mathbf{y}) \times \mathbf{G}_{ij}\right) = \alpha_3 \, \mathbf{e}_x + b_3 \mathbf{e}_y + c_3 \mathbf{e}_z \tag{46}$$

where a_3, b_3, c_3 are known scalar quantities. In this manner, equation (44) can be written in its final form as

$$d_3 = x_{p''} \, a_3 + y_{p''} b_3 + z_{p''} c_3. \tag{47}$$

Equations (34), (40) and (47) define the sought system of three equations with respect to the unknowns $x_{p''},\ y_{p''},\ z_{p''}$

$$\begin{bmatrix} a_1 & b_1 & c_1 \\ a_2 & b_2 & c_2 \\ a_3 & b_3 & c_3 \end{bmatrix} \begin{bmatrix} x_{p''} \\ y_{p''} \\ z_{p''} \end{bmatrix} = \begin{bmatrix} d_1 \\ d_2 \\ d_3 \end{bmatrix}, \tag{48}$$

which leads straightforwardly to a unique solution for $x_{p''},\ y_{p''},\ z_{p''}$.

Computationally, the solution of (48) leads to the definition of a function that needs to be called inside a repetitive loop in order to evaluate the coordinates of all P'' points. This function contains nine known arguments, namely the coordinates of the starting and ending point of each considered segment, as well as the coordinates of point P' of the polyhedral face where the specific segment belongs. The unknown quantities are the coordinates of P''.

The aforementioned repetitive procedure goes first through all of the polyhedral faces and then through each one of the segments building the corresponding polygonal boundary of each face. During this procedure and following the evaluation of the coordinates of point P' the computation of parameter h_{pq} is performed we well, to provide for each segment the distance between points P' and P'' on that face, which is defined from the difference between the corresponding position vectors as

$$h_{pq} = \left\| \mathbf{x}' - \mathbf{x} \right\|. \tag{49}$$

A necessary hypothesis that has to be examined is whether P' lies already on the direction of some segment, thus coincides with P''. In this case, the coordinates of the two points are identical, and the distance between them is zero. This scenario can be controlled through parameter σ_{pq}. Namely, when in the frame of the mentioned loop the condition $\sigma_{pq} = 0$ appears for a specific segment, then the coordinates of P'' are set equal to those of P' and $h_{pq} = 0$.

Computation of singular terms and final expressions

The evaluation of expressions (4)–(6) follows a common computational pattern, the only distinction being the exact analytical definition of the singularity correction terms and final formulas. However, the numerical implementation of the equations or the decision when to insert the singularity terms are common and based on the constant monitoring of the positions of points P' and P'' with respect to the boundaries of the polyhedral source. Potential and first-order derivatives share the definition for the involved corrections when singularities occur, the corresponding terms differ for the second-order derivatives.

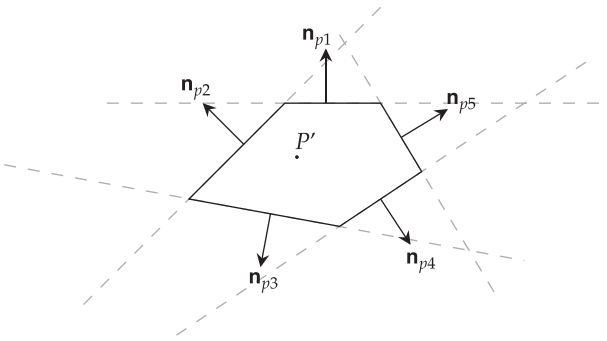

Figure 9 Point P' *located inside the area defined by a polygonal face and related unit normal segments*.

The basic feature of the computational algorithm has already been sketched above: two nested loops, following the definitions of the two summations in (4)–(6), one running through the faces of the polyhedral source and the other through the segments of each face. Thereby, the definition of certain variables can facilitate the monitoring of the position of point P' and consequently define the value of the corresponding correction term. Thus, following variables are defined: variable $\mathrm{SING}_{\mathrm{area}}$ controlling whether P' is located inside the considered face, variable $\mathrm{SING}_{\mathrm{vert}}$ which examines if P' coincides with a vertex and variable $\mathrm{SING}_{\mathrm{segm}}$ which checks whether P' is situated on a polyhedral segment. At the end of the second loop, if any of these indices change in numerical value, P' is located on the specific position of the boundary surface and the evaluation of the corresponding correction terms is due. The subsequent examination of the position of point P'' is again based on the computation of characteristic geometric quantities and leads to the correct determination of the involved distances between P'' and the polyhedral vertices. The final considerations involve the numerical values of the transcendental functions entering expressions (4)–(6) for each of the above special cases.

Position of P′ with respect to the source

The first control for the determination of the relative position of point P' with respect to the polyhedral source involves the possibility that P' lies inside the area defined by the polygonal boundary of the specific face (Fig. 9). Segment unit normals $\mathbf{n}_{pq}$ and parameters σ_{pq} serve this purpose. When, for a specific segment the consideration of σ_{pq} according to definition (28) equals to +1, vector $\mathbf{n}_{pq}$ points to the half plane that does not

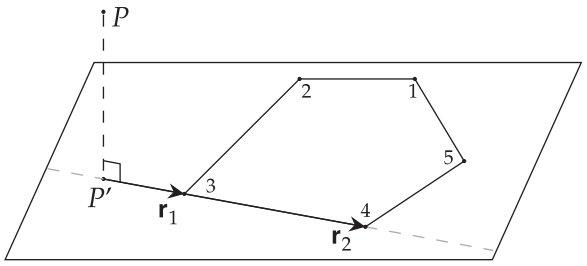

Figure 10 Point P' *on the direction of a polygonal segment.*

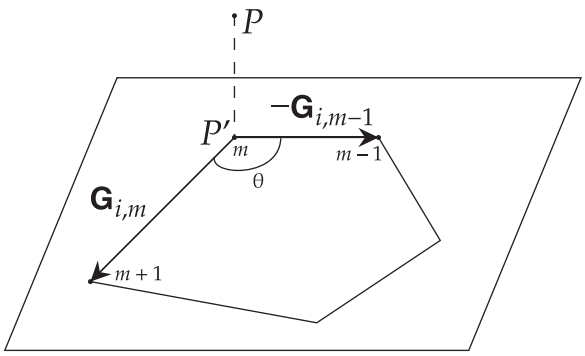

Figure 11 Point P' *coinciding with a polyhedral vertex.*

include P'. Modifying parameter $\mathrm{SING}_{\mathrm{area}}$ every time this is the case according to

$$\mathrm{SING}_{\mathrm{area}} = \mathrm{SING}_{\mathrm{area}} + 1 \tag{50}$$

provides the sought geometric control. Namely, when the examination of all segments of a specific face is completed and the value of parameter $\mathrm{SING}_{\mathrm{area}}$ equals to the total number of segments in that particular face, one concludes that all segment unit normals $\mathbf{n}_{pq}$ point to the opposite direction of P'; consequently, P' lies inside the examined face and the correction terms $\mathrm{SING}_{A_p} = -2\pi h_p$ and $\mathrm{SING}_{B_{pj}} = -2\pi \cos(\boldsymbol{N}_p, \boldsymbol{e}_j)\sigma_p$ have to be evaluated (Tsoulis and Petrovic, 2001).

When $\sigma_{pq} = 0$, i.e. when P' lies on the direction of a segment, a further check has to be performed. This involves the definition of the vectors linking P' with the two segment vertices according to

$$\mathbf{r}_1 = \left(x_{p'_i} - x_{i,j}\right)\,\mathbf{e}_x + \left(y_{p'_i} - y_{i,j}\right)\mathbf{e}_y + \left(z_{p'_i} - z_{i,j}\right)\mathbf{e}_z \tag{51}$$

$$\mathbf{r}_2 = \left(x_{p'_i} - x_{i,j+1}\right)\,\mathbf{e}_x + \left(y_{p'_i} - y_{i,j+1}\right)\mathbf{e}_y + \left(z_{p'_i} - z_{i,j+1}\right)\mathbf{e}_z \tag{52}$$

with $x_{i,j}, y_{i,j}, z_{i,j}$ the coordinates of the vertex in the i face and j position, the latter describing the order of the vertices in the topology file. The comparison of the magnitudes of the two vectors (51) and (52) reveals the actual position of point P' on the direction of the specific segment with respect to its two vertices (Fig. 10).

If one of the magnitudes $\|\mathbf{r}_1\|$ or $\|\mathbf{r}_2\|$ equals to zero, then P' coincides with the corresponding segment vertex as well as with point P''. In this special case, the evaluation of the correction terms $\mathrm{SING}_{A_p} = -\theta h_p$ and $\mathrm{SING}_{B_{pj}} = -\theta \cos(\mathbf{N}_p, \mathbf{e}_j)\sigma_p$ is needed, where θ is the angle between the subsequent segments that meet at the vertex in question. If, for instance point P' coincides with vertex m, then angle θ will be provided by

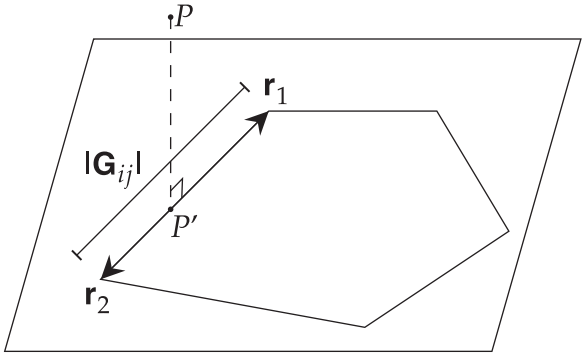

Figure 12 Point P' *located on a polyhedral segment between its vertices.*

segments $m-1$ and $m+1$ through the inner product definition:

$$\theta = \arccos\left(\frac{\mathbf{G}_2 \cdot (-\mathbf{G}_1)}{\|\mathbf{G}_2\|\,\|-\mathbf{G}_1\|}\right), \tag{53}$$

with $\mathbf{G}_1, \mathbf{G}_2$ being the vectors defining the two adjacent segments (see Fig. 11).

Securing that the correction terms $-\theta h_p$ and $-\theta \cos(\mathbf{N}_p, \mathbf{e}_j)\sigma_p$ will be inserted in the final expressions is provided by the insertion in the loop running through the segments of a face of parameter $\mathrm{SING}_{\mathrm{vert}}$, which, when either of r_1 or r_2 equals to zero, is modified as

$$\mathrm{SING}_{\mathrm{vert}} = \mathrm{SING}_{\mathrm{vert}} + 1. \tag{54}$$

When the control of all segments of a face is completed, the terms $-\theta h_p$ and $-\theta \cos(\mathbf{N}_p, \mathbf{e}_j)\sigma_p$ will be inserted as corrections in the final expressions, if $\mathrm{SING}_{\mathrm{vert}} > 0$.

Finally, when $\sigma_{pq} = 0$ and the magnitudes $\|\mathbf{r}_1\|$ and $\|\mathbf{r}_2\|$ are both less than the length of the examined segment $\|\mathbf{G}_{ij}\|$ then P' is located on the segment between its two vertices (Fig. 12). With the addition of the control parameter $\mathrm{SING}_{\mathrm{segm}}$

into the computational algorithm, which in the examined case will be altered according to

$$\mathrm{SING}_{\mathrm{segm}} = \mathrm{SING}_{\mathrm{segm}} + 1, \tag{55}$$

the inclusion of the corresponding correction term is enabled. More precisely, the fact that $\mathrm{SING}_{\mathrm{segm}} > 0$ in the end of going through all segments of a face implies that for the specific face point P' is located on a segment between its vertices and the terms $\mathrm{SING}_{A_p} = -\pi h_p$ and $\mathrm{SING}_{B_{pj}} = -\pi \cos(\mathbf{N}_p, \mathbf{e}_j)\sigma_p$ should be added into the final expressions.

Computation of functions LN_{pq} and AN_{pq}

For the computation of functions LN_{pq} and AN_{pq} one needs to evaluate the four distances $s_{1pq}, s_{2pq}, l_{1pq}, l_{2pq}$. Position vectors $\mathbf{s}$ link the vertices of the segment with point P'', while vectors $\mathbf{l}$ refer to the origin of the local coordinate system, situated at computation point P.

For segment G_{ij}, the above distances are defined as

$$\mathbf{s}_{1pq} = \left(x_{i,j} - x_{P''}\right)\ \mathbf{e}_x + \left(y_{i,j} - y_{P''}\right)\mathbf{e}_y + \left(z_{i,j} - z_{P''}\right)\mathbf{e}_z \tag{56}$$

$$\mathbf{s}_{2pq} = \left(x_{i,j+1} - x_{P''}\right)\ \mathbf{e}_x + \left(y_{i,j+1} - y_{P''}\right)\mathbf{e}_y + \left(z_{i,j+1} - z_{P''}\right)\mathbf{e}_z \tag{57}$$

$$\mathbf{l}_{1pq} = \left(x_{i,j}\right)\ \mathbf{e}_x + \left(y_{i,j}\right)\mathbf{e}_y + \left(z_{i,j}\right)\mathbf{e}_z \tag{58}$$

$$\mathbf{l}_{2pq} = \left(x_{i,j+1}\right)\ \mathbf{e}_x + \left(y_{i,j+1}\right)\mathbf{e}_y + \left(z_{i,j+1}\right)\mathbf{e}_z \tag{59}$$

where $x_{P''}, y_{P''}, z_{P''}$ are the coordinates of P'' for the considered segment, $x_{i,j}, y_{i,j}, z_{i,j}$ are the coordinates of the first and $x_{i,j+1}, y_{i,j+1}, z_{i,j+1}$ are the coordinates of the second vertex.

The assignment of signs to the magnitudes of these vectors depends on the definition of a 1D coordinate system on the direction of the segment with origin point P''. Depending on the relative position of P'' with respect to the two vertices, all aforementioned magnitudes are assigned with the appropriate sign. Thereby, we control the following geometric options:

First option: $\|\mathbf{s}_1\| < \|\mathbf{G}_{ij}\|$ and $\|\mathbf{s}_2\| < \|\mathbf{G}_{ij}\|$. Point P'' is situated inside the examined segment. The origin of the 1D coordinate system on the direction of the segment is placed at P'' and the signs of the computed distances are defined as

$$s_1 = -\|\mathbf{s}_1\|, \quad s_2 = \|\mathbf{s}_2\|, \quad l_1 = \|\mathbf{l}_1\|, \quad l_2 = \|\mathbf{l}_2\|. \tag{60}$$

Second option: In case first hypothesis is discarded one checks whether $\|\mathbf{s}_2\| < \|\mathbf{s}_1\|$. Here, P'' is found on the right side of the considered segment, i.e. closest to the second vertex of the segment, if we consider the order by which the vertices are given in the topology file. Thus, the corresponding distances are assigned with a negative sign as

$$s_1 = -\|\mathbf{s}_1\|, \quad s_2 = -\|\mathbf{s}_2\|, \quad l_1 = \|\mathbf{l}_1\|, \quad l_2 = \|\mathbf{l}_2\|. \tag{61}$$

Third option: The other possibility to be controlled, if the first condition is rejected, is $\|\mathbf{s}_1\| < \|\mathbf{s}_2\|$. Now, P'' is located on the left side of the considered segment and both distances to the two vertices are assigned the positive sign (see Fig. 13)

$$s_1 = \|\mathbf{s}_1\|, \quad s_2 = \|\mathbf{s}_2\|, \quad l_1 = \|\mathbf{l}_1\|, \quad l_2 = \|\mathbf{l}_2\|. \tag{62}$$

Fourth option: An independent scenario occurs when the computation point P is located from the beginning on the direction of a specific segment. In this case, when the loop arrives at that segment P coincides with P' and P''. This setting takes place when

$$\|\mathbf{s}_1\| = \|\mathbf{l}_1\| \quad \text{and} \quad \|\mathbf{s}_2\| = \|\mathbf{l}_2\| \tag{63}$$

or similarly

$$\|\mathbf{s}_1 - \mathbf{l}_1\| = 0 \quad \text{and} \quad \|\mathbf{s}_2 - \mathbf{l}_2\| = 0. \tag{64}$$

When this happens, the three-dimensional distances $\mathbf{l}_{1pq}, \mathbf{l}_{2pq}$ refer to the same 1D coordinate system which is defined on the direction of the segment, thus these distances too will acquire a sign according to the one-dimensional discussion presented above. The cases follow the controls expressed by the three aforementioned hypotheses. The three possibilities are

Case one: Point P lies inside the considered segment. The examined functions are defined as

$$s_1 = -\|\mathbf{s}_1\|, \quad s_2 = \|\mathbf{s}_2\|, \quad l_1 = -\|\mathbf{l}_1\|, \quad l_2 = \|\mathbf{l}_2\|. \tag{65}$$

Case two: Point P is located on the direction of the segment from its right side. The sign attribution becomes

$$s_1 = -\|\mathbf{s}_1\|, \quad s_2 = -\|\mathbf{s}_2\|, \quad l_1 = -\|\mathbf{l}_1\|, \quad l_2 = -\|\mathbf{l}_2\|. \tag{66}$$

Case three: Point P is located on the direction of the segment from its left side. Equation (66) now gives

$$s_1 = \|\mathbf{s}_1\|, \quad s_2 = \|\mathbf{s}_2\|, \quad l_1 = \|\mathbf{l}_1\|, \quad l_2 = \|\mathbf{l}_2\|. \tag{67}$$

IMPLEMENTATION AND VALIDATION

The appended function GPolyhedron.m was developed in Matlab for the implementation of equations (4)–(6) following all of the aforementioned algorithmic steps. For the sake of validation, two test bodies were considered and compared against the existing Fortran code of Tsoulis (2012). The first case study was the distribution of a rectangular parallelepiped

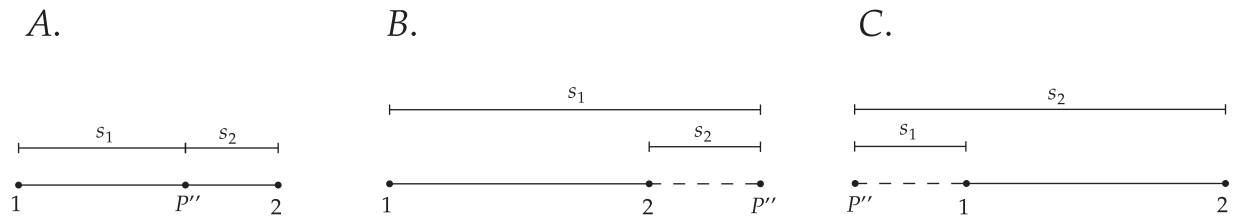

Figure 13 Three hypotheses regarding the sign attribution to the involved distances depending on the position of P'' *on the direction of the examined segment*.

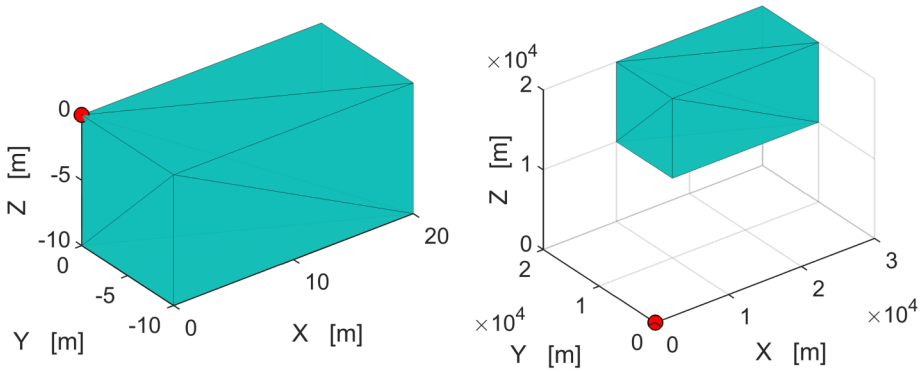

Figure 14 Two characteristic cases, case 1 (left) and case 2 (right), of the examined rectangular parallelepiped distribution. The red dot describes the location of the computation point.

Table 1 Potential and first-order derivatives for the two cases of Figure 14

	Case 1	Case 2
V	$3.19403761604211 \times 10^{-5}$ m^{2}s^{-2}	$1.22929116776966 \times 10$ m^{2}s^{-2}
V_x	$2.31329148957265 \times 10^{-6}$ ms^{-2}	$2.78984765072042 \times 10^{-4}$ ms^{-2}
V_y	$1.91973919943186 \times 10^{-6}$ ms^{-2}	$2.28376978663176 \times 10^{-4}$ ms^{-2}
V_z	$1.91973919943186 \times 10^{-6}$ ms^{-2}	$2.28376978663179 \times 10^{-4}$ ms^{-2}

with constant density 2670 kg m^{-3}, represented by means of a triangular mesh (Fig. 14). A total of 28 different cases were considered, either by changing the dimensions but not the shape of the parallelepiped, or by examining different positions of the computation point with respect to the prismatic source. The former selection aimed to investigate the numerical performance of the method when considering distributions that deviate from a mass point representation, the latter to test the effect of signal attenuation with increasing distance of the computation point from the source.

Tables 1 and 2 present the calculated values for the specific cases included in Figure 14, where the parallelepiped is of dimensions 20 m × 10 m × 10 m and 20 km × 10 km × 10 km, respectively. Table 3 includes the overall statistics for the differences between the present software and that of Tsoulis (2012) for all 28 cases.

For the majority of the tests, an absolute agreement between the two programmes is obtained. In addition, no specific discrepancy is revealed in the differences when altering the distance of the computational point with respect to the source, or when changing the dimensions of the three-dimensional distribution while using the same fixed point. The maximum absolute difference observed is of the order 10^{-16} m^{2}s^{-2} for the gravitational potential, 10^{-19} m s^{-2} for the first-order derivatives and 10^{-21} s^{-2} for the second-order derivatives.

The irregularly shaped asteroid 433 Eros, which was mapped by the NEAR Shoemaker probe (Zuber et al, 2000), was selected as the second test body for the numerical validation of GPolyhedron.m (Fig. 15). The asteroid has an approximate size of 13 km × 13 km × 33 km, while the same constant density of 2670 kg m^{-3} was used, as its choice is irrelevant for the present investigations. Again, an abundance of cases was

Table 2 Second-order potential derivatives for the two cases of Figure 14

	Case 1		
V_{ij} [s^{-2}]	$-3.58735552599256 \times 10^{-8}$	$7.97910192187069 \times 10^{-8}$ $-1.21988308530518 \times 10^{-7}$	$7.97910192187069 \times 10^{-8}$ $7.97910192187069 \times 10^{-8}$ $-1.21988308530518 \times 10^{-7}$
	Case 2		
V_{ij} [s^{-2}]	$3.77145169819759 \times 10^{-9}$	$1.54879774341877 \times 10^{-8}$ $-1.88572584909883 \times 10^{-9}$	$1.54879774341877 \times 10^{-8}$ $1.33659538654055 \times 10^{-8}$ $-1.88572584909884 \times 10^{-9}$

Table 3 Differences between GPolyhedron.m and the Fortran code in Tsoulis (2012) for the ensemble of the considered 28 cases for the rectangular parallelepiped

	Average	Min	Max	Std
V	-3.420×10^{-17} m^2s^{-2}	-9.992×10^{-16} m^2s^{-2}	3.133×10^{-17} m^2s^{-2}	1.928×10^{-16} m^2s^{-2}
V_i	4.502×10^{-21} ms^{-2}	-3.956×10^{-19} ms^{-2}	3.015×10^{-19} ms^{-2}	6.463×10^{-20} ms^{-2}
V_{ij}	1.189×10^{-24} s^{-2}	-7.091×10^{-21} s^{-2}	2.965×10^{-21} s^{-2}	6.591×10^{-22} s^{-2}

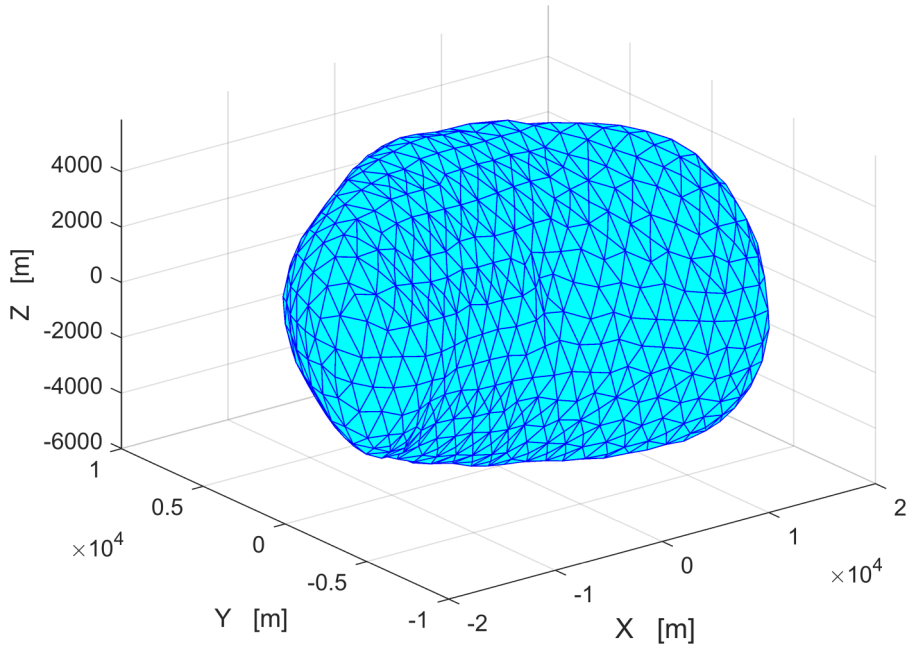

Figure 15 The arbitrarily shaped source of asteroid 433 Eros, used as the second test distribution for the numerical validation of GPolyhedron.m.

selected for different locations of the computation point, all of which led to the verification of the aforementioned numerical agreement obtained for the first test body. Table 4 presents the numerical results for two computation points selected to coincide with two of the asteroid's vertices but at a different distance from its centre of mass.

The aforementioned agreement between the two codes is verified for these computations as well. Overall, all

Table 4 Differences between GPolyhedron.m and the Fortran code in Tsoulis (2012) for two computation points coinciding with two vertices of asteroid Eros having varying distance from its centre of mass

Computation point		Distance from asteroid's centre of mass	
X	−17075.3	17303.150	
Y	−2763.85		
Z	440.763		
	GPolyhedron.m	Tsoulis (2012)	Difference
V	$3.42850254599056 \times 10$	$3.42850254599058 \times 10$	$-2.06057393370429 \times 10^{-13}$
Vx	$3.69513991852252 \times 10^{-3}$	$3.69513991852252 \times 10^{-3}$	0.00000000000000
Vy	$2.07017660762558 \times 10^{-3}$	$2.07017660762556 \times 10^{-3}$	$1.99493199737333 \times 10^{-17}$
Vz	$3.53891625473671 \times 10^{-4}$	$3.53891625473700 \times 10^{-4}$	$-2.90024081139872 \times 10^{-17}$
Vxx	$-3.51713847304506 \times 10^{-6}$	$-3.51713847304506 \times 10^{-6}$	0.00000000000000
Vyy	$3.31694607335281 \times 10^{-7}$	$3.31694607335279 \times 10^{-7}$	$2.01170324972896 \times 10^{-21}$
Vzz	$1.18725862153571 \times 10^{-7}$	$1.18725862153571 \times 10^{-7}$	0.00000000000000
Vxy	$2.76540793293196 \times 10^{-8}$	$2.76540793293184 \times 10^{-8}$	$1.20106624942700 \times 10^{-21}$
Vxz	$-1.04380954506278 \times 10^{-5}$	$-1.04380954506278 \times 10^{-5}$	0.00000000000000
Vyz	$6.95204349247191 \times 10^{-6}$	$6.95204349247191 \times 10^{-6}$	0.00000000000000
Computation Point		Distance from asteroid's center of mass	
X	5791.62	8520.295	
Y	−3922.51		
Z	−4864.82		
	GPolyhedron.m	Tsoulis (2012)	Difference
V	$5.02566664319091 \times 10$	$5.02566664319091 \times 10$	0.00000000000000
Vx	$1.07604380017073 \times 10^{-4}$	$1.07604380017079 \times 10^{-4}$	$-6.00376953013848 \times 10^{-18}$
Vy	$3.06188120810973 \times 10^{-3}$	$3.06188120810971 \times 10^{-3}$	$2.03830008427275 \times 10^{-17}$
Vz	$4.46958367423344 \times 10^{-3}$	$4.46958367423340 \times 10^{-3}$	$3.98986399474666 \times 10^{-17}$
Vxx	$-3.88296293487037 \times 10^{-6}$	$-3.88296293487038 \times 10^{-6}$	$1.01643953670516 \times 10^{-20}$
Vyy	$5.55591495436341 \times 10^{-6}$	$5.55591495436340 \times 10^{-6}$	$9.31736241979730 \times 10^{-21}$
Vzz	$-4.52111199701719 \times 10^{-7}$	$-4.52111199701715 \times 10^{-7}$	$-3.97046694025453 \times 10^{-21}$
Vxy	$2.26948445900768 \times 10^{-6}$	$2.26948445900768 \times 10^{-6}$	0.00000000000000
Vxz	$-5.27712813952077 \times 10^{-7}$	$-5.27712813952080 \times 10^{-7}$	$2.96461531539005 \times 10^{-21}$
Vyz	$-6.68601757791733 \times 10^{-7}$	$-6.68601757791738 \times 10^{-7}$	$4.97631856511901 \times 10^{-21}$

gravity functionals are numerically identical for both considered test distributions at the level of the significant decimal digits precision of the double-precision floating point format.

SUMMARY AND CONCLUDING REMARKS

The linear integral approach for the polyhedral gravity signal is a flexible analytical solution for computing the gravitational potential function, its first- and second-order derivatives due to a polyhedral attracting source. Apart from offering an exact solution to the problem in hand, the key property of the method is that it describes generally shaped polyhedra, i.e. polyhedral sources where the triangulation algorithm is allowed to vary the number of segments between different faces. This feature permits the modelling of arbitrarily complex distributions setting no limitations to the range of applications. At the same time, the method concludes to the evaluation of transcendental functions of position, which are computationally demanding, especially when applied to larger data sets.

The method has a strong geometric profile. As it pursues a straightforward analytical solution of the corresponding three-dimensional integral expressions, it utilizes a consecutive application of the divergence theorem until it breaks down the volume integrals into line integrals defined along the polyhedral edges, that have closed solutions. This approach inevitably involves the definition of numerous coordinate systems, following the projection of the computation point onto the different faces and individual segments along the specific polygonal boundaries. Another consequence of this computational strategy is that for certain positions of the involved points with respect to the attracting source, the approach requires the numerical evaluation of correction terms, which

counteract for the fact that the application of the divergence theorem is singular at these points.

The mathematical structure of the method has specific geometric consequences. Using standard vector calculus tools, a constant monitoring of the positions of all characteristic points (computation point and its necessary projections) is required. Furthermore, the topology file including the connectivity information of the vertices of the examined source has to fulfil the geometric prerequisite that the vertices for each face should be ordered in such a way that an outward-pointing face unit normal is defined. Finally, the definition of different coordinate systems at each segment inserts additional controls in the algorithm, as distances, which enter all involved transcendental functions, require to get assigned the appropriate signs in the corresponding 1D coordinate systems.

The present contribution aims to cover all of these aspects and offer a complete geometric insight into the line integral approach for the analytical computation of the gravity signal of an arbitrarily shaped polyhedral source. The appended code implements all geometric considerations in detail, validates independently the available code and offers an additional flexible tool in gravity modelling and interpretation.

ELECTRONIC SUPPLEMENT

GPolyhedron.m with all necessary input files used for the validation tests of Section 4 are available through repository https://github.com/Gavriilidou/GPolyhedron. The shape of asteroid Eros is freely available from the Small Bodies Node of the Planetary Science Institute at https://sbn.psi.edu/pds/shape-models/.

DATA AVAILABILITY STATEMENT

Data sharing is not applicable to this article as no new data were created or analysed in this study.

REFERENCES

Barnett, C.T. (1976) Theoretical modeling of the magnetic and gravitational fields of an arbitrary shaped three-dimensional body. *Geophysics*, 41, 1353–1364.

Benedek, J., Papp, G. and Kalmár, J. (2018) Generalization techniques to reduce the number of volume elements for terrain effect calculations in fully analytical gravitational modelling. *Journal of Geodesy*, 92(4), 361–381.

Bucha, B., Janák, J., Papčo, J. and Bezdek, A. (2016) High-resolution regional gravity field modelling in a mountainous area from terrestrial gravity data. *Geophysical Journal International*, 207(2), 949–966.

Capponi, M., Mansi, A.H. and Sampietro, D. (2018) Improving the computation of the gravitational terrain effect close to ground stations in the GTE software. *Studia Geophysica et Geodaetica*, 62(2), 206–222.

Chanut, T.G.G., Aljbaae, S., Prado, A.F.B.A. and Carruba, V. (2017) Dynamics in the vicinity of (101955) Bennu: solar radiation pressure effects in equatorial orbits. *Monthly Notices of the Royal Astronomical Society*, 470(3), 2687–2701.

D'Urso, M.G. (2013) On the evaluation of the gravity effects of polyhedral bodies and a consistent treatment of related singularities. *Journal of Geodesy*, 87(3), 239–252.

D'Urso, M.G. (2014) Gravity effects of polyhedral bodies with linearly varying density. *Celestial Mechanics and Dynamical Astronomy*, 120(4), 349–372.

D'Urso, M.G. and Trotta, S. (2017) Gravity anomaly of polyhedral bodies having a polynomial density contrast. *Surveys in Geophysics*, 38(4), 781–832.

Fukushima, T. (2017) Precise and fast computation of the gravitational field of a general finite body and its application to the gravitational study of asteroid Eros. *Astronomical Journal*, 154(4), 145

Götze, H.J. and Lahmeyer, B. (1988) Application of three-dimensional interactive modeling in gravity and magnetics. *Geophysics*, 53, 1096–1108.

Hansen, R.O. (1999) An analytical expression for the gravity field of a polyhedral body with linearly varying density. *Geophysics*, 64, 75–77.

Holstein, H. (2003) Gravimagnetic anomaly formulas for polyhedra of spatially linear media. *Geophysics*, 68, 157–167.

Holstein, H. and Ketteridge, B. (1996) Gravimetric analysis of uniform polyhedra. *Geophysics*, 61, 357–364.

Jiang, Y., Baoyin, H. and Yang, M. (2018) Dynamical model of binary asteroid systems using binary octahedrons. *Journal of Astrophysics and Astronomy*, 39(5), 54

Okabe, M. (1979) Analytical expressions for gravity anomalies due to homogeneous polyhedral bodies and translations into magnetic anomalies. *Geophysics*, 44, 730–741.

Petrovic, S. (1996) Determination of the potential of homogeneous polyhedral bodies using line integrals. *Journal of Geodesy*, 71(1), 44–52.

Pohánka, V. (1988) Optimum expression for computation of the gravity field of a homogeneous polyhedral body. *Geophysical Prospecting*, 36, 733–751.

Ren, Z., Chen, C., Zhong, Y., Chen, H., Kalscheuer, T., Maurer, H., et al. (2020) Recursive analytical formulae of gravitational fields and gradient tensors for polyhedral bodies with polynomial density contrasts of arbitrary non-negative integer orders. *Surveys in Geophysics*, 41(4), 695–722.

Ren, Z., Zhong, Y., Chen, C., Tang, J., Kalscheuer, T., Maurer, H. and Li, Y. (2018) Gravity gradient tensor of arbitrary 3D polyhedral bodies with up to third-order polynomial horizontal and vertical mass contrasts. *Surveys in Geophysics*, 39(5), 901–935.

Saraswati, A.T., Cattin, R., Mazzotti, S. and Cadio, C. (2019) New analytical solution and associated software for computing

full-tensor gravitational field due to irregularly shaped bodies. *Journal of Geodesy*, 93(12), 2481–2497.

Schmidt, S., Plonka, C., Götze, H.J. and Lahmeyer, B. (2011) Hybrid modelling of gravity, gravity gradients and magnetic fields. *Geophysical Prospecting*, 59(6), 1046–1051.

Singh, B. and Guptasarma, D. (2001) New method for fast computation of gravity and magnetic anomalies from arbitrary polyhedral. *Geophysics*, 66, 521–526.

Tsoulis, D. (2003) Terrain modeling in forward gravimetric problems: a case study on local terrain effects. *Journal of Applied Geophysics*, 54(1–2), 145–160.

Tsoulis, D. (2012) Analytical computation of the full gravity tensor of a homogeneous arbitrarily shaped polyhedral source using line integrals. *Geophysics*, 77(2), F1–F11.

Tsoulis, D. and Petrovic, S. (2001) On the singularities of the gravity field of a homogeneous polyhedral body. *Geophysics*, 66(2), 535–539.

Vitale, A. and Fedi, M. (2020) Inversion of potential fields with an inhomogeneous depth weighting function. SEG International Exposition and Annual Meeting (2019), 1749–1753.

Werner, R.A. (1994) The gravitational potential of a homogeneous polyhedron. *Celestial Mechanics and Dynamical Astronomy*, 59(3), 253–278.

Werner, R.A. and Scheeres, D.J. (1997) Exterior gravitation of a polyhedron derived and compared with harmonic and mascon gravitation representations of asteroid 4769 Castalia. *Celestial Mechanics and Dynamical Astronomy*, 65(3), 313–344.

Zhang, Y. and Chen, C. (2018) Forward calculation of gravity and its gradient using polyhedral representation of density interfaces: an application of spherical and ellipsoidal topographic gravity effect. *Journal of Geodesy*, 92(2), 205–218.

Zuber, M.T., Smith, D.E., Cheng, A.F., Garvin, J.B., Aharonson, O., Cole, T.D., et al. (2000) The shape of 433 Eros from the NEAR-Shoemaker Laser Rangefinder. *Science*, 289, 2097–2101.